Effect of Surface Chemistry and Associated Protein Corona on the Long-Term Biodegradation of Iron Oxide Nanoparticles *In Vivo*

Grazyna Stepien,[1,‡] María Moros,[1,2,‡,] Marta Pérez-Hernández,[1,3] Marta Monge,[4,5] Lucía Gutiérrez,[1] Raluca M. Fratila,[6] Marcelo de las Heras,[7] Sebastián Menao Guillén,[8] Juan José Puente Lanzarote,[8] Conxita Solans,[4] Julián Pardo,[1,3,9] and Jesús Martínez de la Fuente.[6,10,*]*

1-Institute of Nanoscience of Aragon (INA), University of Zaragoza, 50018 Zaragoza, Spain

2- Institute of Applied Sciences and Intelligent Systems-CNR, Via Campi Flegrei, 34, 80078, Pozzuoli, Italy

3- Aragón Health Research Institute (IIS Aragón), Biomedical Research Centre of Aragón (CIBA), 50009 Zaragoza, Spain

4- Institute of Advanced Chemistry of Catalonia (IQAC-CSIC) and CIBER in Bioengineering, Biomaterials and Nanomedicine (CIBER-BBN), Jordi Girona 18-26, Barcelona 08034

5- Department of Pharmacy and Pharmaceutical Technology and Physical Chemistry, University of Barcelona, Av/Joan XXIII s/n, 08028 Barcelona, Spain

6- Aragon Materials Science Institute (ICMA), CSIC-University of Zaragoza and CIBER-BBN, C/Pedro Cerbuna 12, 50009 Zaragoza, Spain

7-Department of Animal Pathology, Veterinary Faculty, University of Zaragoza, 50009 Zaragoza, Spain

8-Department of Clinical Biochemistry. H.C.U. Lozano Blesa, Zaragoza 50009, Spain.

9- ARAID foundation, 50018 Zaragoza, Spain

10-Institute of NanoBiomedicine and Engineering, Shanghai Jiao Tong University, Dongchuan Road 800, 200240 Shanghai, PR China

ABSTRACT: Protein corona formed on the surface of nanoparticle in biological medium determines its behavior *in vivo*. Here, iron oxide nanoparticles containing the same core and shell, but bearing two different surface coatings, either glucose or poly(ethylene glycol), were evaluated. The nanoparticles protein adsorption, *in vitro* degradation, and *in vivo* biodistribution and biotransformation over four months, were investigated. Although both types of nanoparticles bound similar amount of proteins *in vitro*, the differences in the protein corona composition correlated to the nanoparticles biodistribution *in vivo*. Interestingly, *in vitro* degradation studies demonstrated faster degradation for nanoparticles functionalized with glucose, whereas the *in vivo* results were opposite with accelerated biodegradation and clearance of the nanoparticles functionalized with poly(ethylene glycol). Therefore, the variation in the degradation rate observed *in vivo* could be related not only to the molecules attached to the surface, but also with

the associated protein corona, as the key role of the adsorbed proteins on the magnetic core degradation has been demonstrated *in vitro*.

KEYWORDS: iron oxide nanoparticles, protein corona, biodistribution, nanoparticles degradation, *in vivo*

INTRODUCTION

Up to day, iron oxide nanoparticles (IONPs) are one of the most studied nanomaterials for biomedical applications. The considerable interest in IONPs results from the combination of their unique magnetic properties, low toxicity and biodegradability.[1] Therefore, they present a great potential for prominent nanomedicine applications such as external manipulation using magnets, multimodal imaging, triggered drug delivery or hyperthermia induced tumor ablation.[2,3] However, satisfactory employment of nanoparticles (NPs) in any of those applications has not been achieved yet mainly due to one hindrance, that is, controlling the behavior of NPs *in vivo*. Once a NP is administered *in vivo*, it interacts with the components of the physiological environment, specially with proteins, resulting in the formation of so-called protein corona (PC).[4] PC can dramatically change the nanomaterial size, aggregation state and interfacial properties, dominating in an uncontrolled way the biological behavior of NPs.[5]

Although to date it is widely accepted that the presence of this PC would ultimately determine the fate of the nanomaterial, its role in the biotransformation and degradation of NPs *in vivo* has been scarcely investigated.[6] *In vitro*, it has been shown that the PC can enter the cell attached to the NP, and later on, depending on the associated proteins, be destroyed with

different kinetics in the lysosomes.[7] *In vivo,* it is known that once NPs are trapped in cells, their biodegradation process would greatly depend on different factors such as the capping agent, the clustering state or the recycling capacity of the organ.[8,9] Only recently, a comparative study of two different coating shells for gold/iron heterostructures has demonstrated that poly(ethylene glycol) (PEG)-coated NPs were more vulnerable to degradation *in vitro* and *in vivo* than those NPs coated with oleic acid and a polymer, suggesting that this coating, and therefore the associated PC would have a protective role in the degradation of the NPs.[8] However, the composition of the shell was different between both types of NPs, and therefore, the role of the diverse PCs cannot be clearly established.

Here, we provide evidence that the PC is the main responsible for the NPs fate and it is implicated in the NPs degradation process. We report how the surface modification of identical 12 nm IONPs with either glucose or PEG affects the PC identity, the NPs biodistribution and more importantly, the degradation over time.

RESULTS AND DISCUSSION

IONPs synthesis and functionalization

IONPs were synthesized following a previously reported seed-mediated growth method based on the thermal decomposition of Fe(III) acetylacetonate,[10] as this method renders NPs with well-controlled size and high crystallinity. In this case, 12 nm NPs were selected for the *in vivo* studies (Fig. S1) as this diameter will likely avoid renal clearance,[11] allowing to track their biodistribution *in vivo*. The synthesis method provides NPs dispersed in an organic solvent, therefore a subsequent transfer to aqueous solution is required. For this purpose, modification of

a previously reported protocol was applied, where NPs were coated with an amphiphilic polymer shell (poly(maleic anhydride-alt-1-octadecene), PMAO).[12,13,14] Using this methodology, the hydrophobic backbone of the polymer intercalates with the oleic acid chains that covers the NPs core, leaving carboxylic groups exposed to the solvent. In this case, to be able to track the NPs *ex vivo*, they were transferred into water using the PMAO polymer previously modified with a fluorophore, 5-carboxytetramethylrhodamine (TAMRA) (NPs@PMAO, Scheme S1).[15] To provide stability in biological media, NPs@PMAO were functionalized with either glucose (NP@Glc) or PEG molecules (NPs@PEG), as those molecules have been previously demonstrated to efficiently passivate NPs surface avoiding aggregation in cell culture medium *in vitro*.[16,17,18] There is a general consensus that protein adsorption and consequently biodistribution is highly dependent on the PEG molecular weight, therefore a long PEG of 5000 Da was chosen to passivate the surface of the NP. In fact it has been described that maximal reduction in protein adsorption is found for a PEG of 5000 Da.[19] Other examples have also linked this PEG MW with the protein adsorption and consequently with the macrophage uptake. For instance, magnetic NP uptake by macrophages is higher for NPs coated with a PEG of 600 Da when compared to a PEG of 3000 Da.[20]

It should be highlighted that NPs@Glc and NPs@PEG presented the same core size (Fig. S2a), shell structure and stability (in water, phosphate buffered saline or cell culture medium supplemented with 10% bovine serum), differing only in surface properties (Fig. S2b and S3). Therefore, these NPs were perfect candidates for an *in vivo* behavior comparative study, as in this case the adsorption of proteins and macrophage uptake would not be associated with the size of the NPs as previously reported.[21]

Associated protein corona characterization

Before performing *in vivo* experiments, all three NPs types were incubated with serum proteins to form a PC, and further characterized to confirm the adsorption of proteins (Fig. S4). Protein quantification assay revealed that functionalization of the NP surface with either glucose or PEG molecules reduced significantly the amount of non-specifically adsorbed proteins in respect to the un-functionalized NPs@PMAO (Fig. 1a). This is of the highest importance, as the biodistribution and NP pharmacokinetic behavior *in vivo* can be strongly affected by the unspecific adsorption of plasma proteins.[22,23] To determine the identity of the attached PC, the proteins were eluted from the surface of the NP, tryptic digested and the peptides were analyzed by mass spectrometry (LC-MS/MS). 372 different proteins were identified, and the specific proteins adsorbed to each NP and overlapping between them detected (Table S1-S4 and Fig. S5a) We next used the ingenuity pathway analysis software (IPA) for molecular and cellular function analysis for the identified unique proteins adsorbed to NPs@PEG and NPs@Glc. 29 specific proteins adsorbed to NPs@PEG were mapped into 20 molecular and cellular functions (p value < 0.05), while 45 unique proteins absorbed to NPs@Glc were mapped into 28 molecular and cellular functions (p value < 0.05) (Table S5). We used the Venn diagram to evaluate those functions, which were specific for each type of NPs, and those functions that were common for both type of NPs. We observed 20 common molecular and cellular functions (Fig. S5b). Proteins absorbed to NPs@Glc mapped into 8 specific molecular and cellular functions. Further, and in order to investigate if the proteins bound onto NPs may be implicated in governing NP fate, the 372 proteins detected by mass spectrometry were grouped according to their physiological function using UniProt database (Fig. 1b and Fig. S6).

The protein amounts were semi-quantitatively assessed by applying the spectral-counting method (SpC) in order to obtain the percentage of participating proteins in the PC composition (relative abundance). The normalized SpC amounts of each protein, which were identified in the LC-MS/ MS study, were calculated by applying the following equation:[24,25]

$$NpSpCk = \left(\frac{\left({SpC}/{(Mw)_k} \right)}{\sum_{i=1}^{n} \left({SpC}/{(Mw)_i} \right)} \right) X\ 100$$

where NpSpCk is the normalized percentage of the spectral count for protein k, SpC is the identified spectral count, and Mw is the molecular weight (in kDa) of the protein k. This correction takes into account the protein size and evaluates the actual contribution of each protein reflecting its relative protein abundance in the protein corona (Fig. 1b and Fig. S6).

Interestingly, it was shown that although both types of functionalized NPs adsorbed similar amounts of proteins *in vitro*, NPs@Glc adsorbed more proteins considered opsonins (e.g. complement proteins, apolipoproteins). Indeed, a clear difference can be seen in the enrichment of complement components, which promotes clearance of NPs *via* interaction with macrophage complement receptors (Figure S6(a)).[26] In fact the relative abundance is two times higher for NPs@Glc than for NPs@PEG. Fibronectin, also enriched in the PC of NPs@Glc when compared to the PC of NPs@PEG, has been also associated with an uptake by Kupffer cells.[27] Further, specific proteins considered opsonins (coagulation factor XI, mannose-binding protein C, C4b and fibrinogen) were only found in the PC of NPs@Glc. On the other hand, the relative abundance of proteins belonging to the coagulation and apolipoproteins group were comparable (Figure S6(b-c)). Among all detected acute phase proteins, NPs@PEG were found to bind more

α-2-HS-glycoprotein than NPs@Glc (Figure S6(d)). This protein has been described as a negative acute phase reactant with strong analogy to albumin, therefore, it is expected that it will act similarly, promoting elongation of NP circulation in the blood.[27] Lastly, the corona of NPs@PEG was more enriched in albumin (dysopsonin), and other proteins such as kininogen that are associated with NPs covered with a high density of PEG.[21] The enrichment of other components such as clusterin that is thought to be a "don't-eat-me" protein has been found to be similar in both coronas.[28] Although the precise effect of PC composition on NP fate *in vivo* remains unclear, proteins considered opsonins are thought to enhance recognition and uptake of NPs by macrophages resulting in their accumulation in the organs of mononuclear phagocyte system (MPS), mainly in the liver and spleen.[29] Conversely, dysopsonins increase the half-life of molecules in the blood.[27]

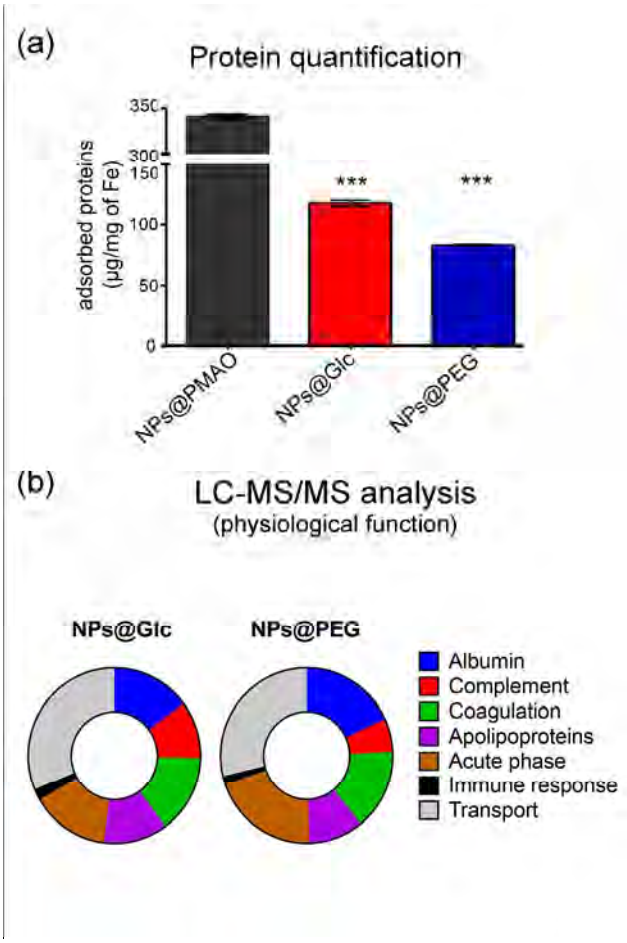

Figure 1. Characterization of the proteins adsorbed to the NPs. (a) Quantitative analysis of the PC bound onto NPs@PMAO, NPs@Glc and NPs@PEG performed using Bicinchonic Acid (BCA)-assay. Black asterisks indicate NPs where the amount of adsorbed proteins is statistically different to the unfunctionalized NPs@PMAO ($p < 0.001$); ordinary one-way ANOVA, Dunnett's multiple comparisons test). (b) Relative abundance of the proteins adsorbed on NPs@Glc and NPs@PEG. The proteins were classified according to their physiological function: albumin; coagulation proteins; complement proteins; apolipoproteins; acute phase proteins; immune response proteins; transport proteins.

In order to verify if the slight variation in the PC composition between NPs@Glc and NPs@PEG was correlated with their biodegradation and biological performance, a complete biodegradation

study was performed *in vitro* and *in vivo*. *In vivo,* the biodistribution of the NPs was previously assessed.

In vitro degradation study

In order to investigate if PC may be implicated in the degradation process, it was decided to use the unfunctionalized NPs, covered just with the polymer (NPs@PMAO) for the *in vitro* degradation study. The PC of those NPs is composed of a much higher amount of proteins than the one of the NPs@Glc or NPs@PEG (Fig. 1a), therefore it was supposed that the effect on the degradation should be more pronounced. NPs@PMAO with and without formed PC (NPs@PMAO-PC and NPs@PMAO, respectively) were incubated in a medium mimicking intracellular lysosomal environment (pH 4.7, 20 mM citrate)[30] or in water (control). Afterwards, NPs were analyzed using transmission electron microscopy (TEM) and alternating current (AC) magnetic measurements. Whereas the first technique allows visual analysis of degradation process, AC magnetic measurements especially through the analysis of the out-of-phase susceptibility ($\chi''(T)$) profile, constitute a powerful tool for both detection (see NPs biodistribution 72 h post-injection section) and over time biotransformation studies. The reduction of the $\chi''(T)$ maximum height, when plotted *per* mass of sample, is an indicator of the decrease of the NPs concentration in a given sample (Fig. 2a).[31] The shift of the $\chi''(T)$ maximum location towards lower temperatures indicates the transformation of the iron core (Fig. 2b). Although there are other parameters that may influence the location in temperature of the $\chi''(T)$ maximum, in this case, the main factor associated to this transformation is the reduction of the particle size due to the degradation process.[32,33]

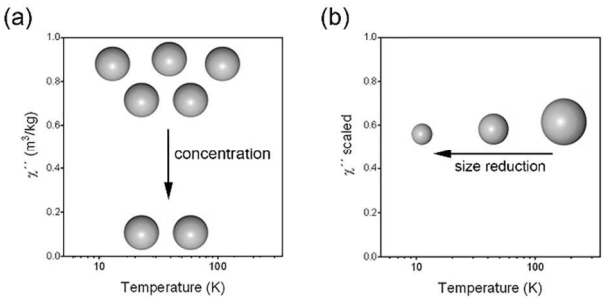

Figure 2. AC magnetic measurements schematic diagram. (a) Schematic representation of the processes associated to a reduction of the χ″(T) maximum height, indicating a decrease of the amount of NPs in a given sample. (b) Schematic representation of the process associated to a shift of the χ″(T) towards lower temperatures: reduction of the NPs core size.

TEM observations showed that NPs@PMAO incubated in the lysosomal medium were degraded, in contrast to their PC-counterparts or the samples in water, that remained unalterable (Fig. 3a). Magnetic measurements (Fig. 3b) confirmed those results as the scaled χ″(T) maximum of the NPs@PMAO incubated in the lysosomal medium was clearly shifted towards lower temperatures on the contrast to other samples. Therefore, these results unambiguously demonstrate that the presence of PC on the surface of NPs provides protection against NP core degradation in the lysosomal medium. Detailed investigation of the degraded NPs showed that NP core, although partially degraded, still maintained the crystalline structure. The dissolved iron ions were retained around NP core as a ring, (Fig. 3c, d) most probably forming coordination complexes with the carboxylic groups of the polymer (Fig. S7). The impact of different accessibility of iron chelating agents to the iron oxide crystal on the degradation kinetics has been already highlighted.[34,35] In this study nanocubes coated with PEG-gallol directly anchored to the iron oxide surface were found to degrade more rapidly and dissolve completely on the

contrast to the nanocubes embedded in an amphiphilic polymer shell similar to the one used here. This was explained by the fact that the polymer chains attached to discrete sites of the crystal surface could leave more access to the small citrate ions provoking accelerated degradation.

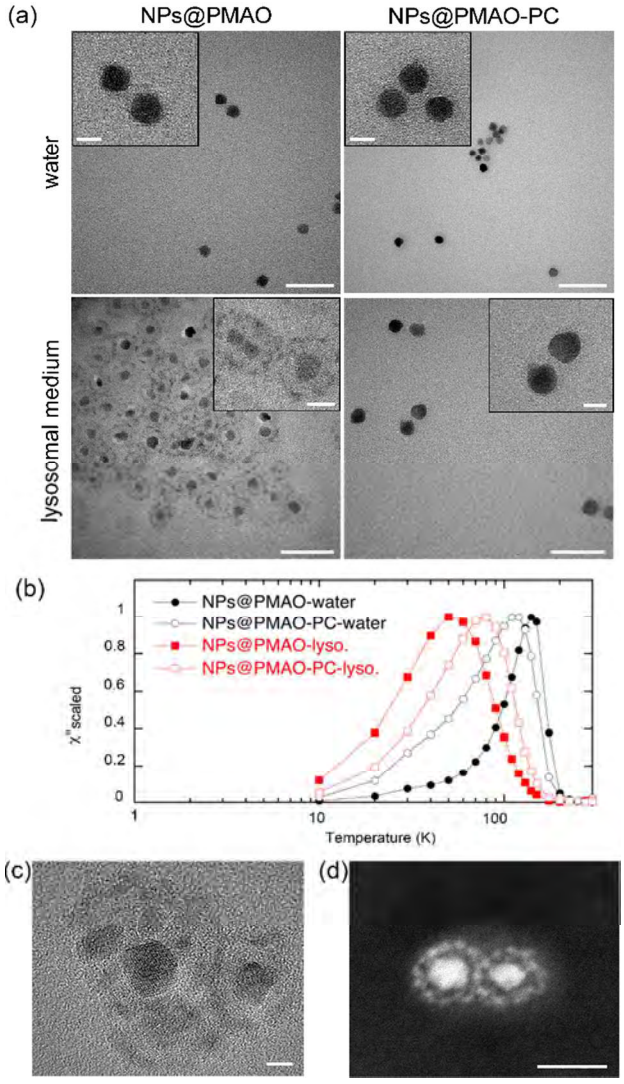

Figure 3. *In vitro* degradation study of NPs@PMAO and NPs@PMAO-PC. (a) Representative TEM micrographs of the NPs@PMAO and NPs@PMAO-PC after incubation in water (upper row) and in lysosomes-mimicking medium (lower row). Scale bar 50 nm, scale bar of the insets 10 nm. (b) Temperature dependence of the out-of-phase component of the AC magnetic susceptibility from NPs@PMAO and NPs@PMAO-PC incubated in the lysosomal medium (-

lyso) or in water (control). (c) High Resolution-TEM micrograph of NPs@PMAO incubated in the lysosomal mimicking medium. Scale bar: 5 nm. (d) Scanning transmission electron microscope mode imaging of the same NPs. Scale bar: 20 nm.

Further, to investigate if the differences in the PC composition between NPs@Glc and NPs@PEG influence on the degradation rate, both NPs types with PC were incubated in a lysosomal mimicking medium as described before. It was found by TEM that in only ten days of incubation, a significant part of the NPs@Glc was totally degraded losing their original shape, while most of the NPs@PEG remained unaffected (Fig. 4a). Those results were also confirmed by the AC magnetic measurements (Fig. 4b). Here the signal for NPs@Glc incubated in acidic medium was clearly moved towards lower temperatures on the contrary to the NPs@PEG one, indicating that the core of the first type of NPs has been modified.

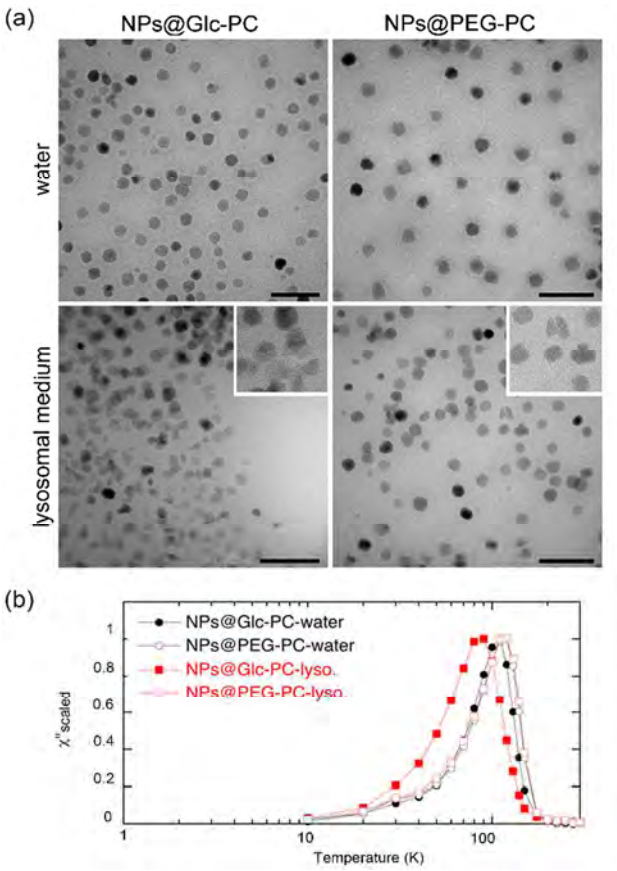

Figure 4. *In vitro* degradation study of NPs@Glc and NP@PEG with their formed PCs (NPs@Glc-PC and NPs@PEG-PC, respectively). (a) Representative TEM micrographs of the NPs@Glc-PC and NPs@PEG-PC after incubation in water (upper row) and in lysosomes-mimicking medium (lower row). Scale bar: 50 nm. (b) Temperature dependence of the out-of-phase component of the AC magnetic susceptibility from NPs@Glc-PC and NPs@PEG-PC incubated in the lysosomal medium (-lyso) or in water (control).

Those results are quite interesting, as both NPs types although are composed of exactly the same core and shell structure (Fig. S2a), present diverse degradation profiles *in vitro*. These results can be explained by the fact that as already described in the literature,[36] the capping agents (in this

case glucose and PEG molecules used for the functionalization), influence on the different accessibility to the iron surface. In fact, also in this study we found that the NPs@Glc and NPs@PEG not bearing their PCs degraded with different kinetics *in vitro* (Fig. S8). However, the NPs@Glc without the adsorbed PC were found to be degraded to a greater extent than the same NPs bearing PC. By comparing TEM micrographs, it can be noticed that although some part of NPs@Glc-PC was degraded in the acidic environment, another part of those NPs preserved quite good their original morphology (Fig. 4a left upper corner of the NPs@Glc-PC/lysosomal medium micrograph). On the other hand, almost all NPs@Glc incubated in the lysosomal medium were found degraded. Concordantly, the scaled $\chi''(T)$ maximum of the NPs@Glc-PC incubated in the acidic medium was shifted only to 90 K, whereas the same signal but for the NPs@Glc incubated in the acidic medium reached 40 K. Therefore, also in this case it was found, that PC can provide at least partial protection against degradation of the NP core.

Interestingly, recent studies indicate that the accessibility to the iron surface may not only depend on the capping agent, but also on the composition of PC. In fact, proteins attached to the NPs can be digested in the lysosomal environment with different kinetics.[7] It has been suggested that proteins of lower molecular weight would be degraded slower than others with higher molecular weights.[37] Taking into account that both the attached molecule and the PC have an effect in the biodegradation *in vitro*, NPs@Glc and NPs@PEG were administrated *in vivo* to verify the biodistribution and biodegradation of NPs.

In vivo biodistribution and toxicity study

Despite the fact that IONPs are considered biocompatible, their safety may vary depending on different factors, such as: composition, physicochemical properties, route of administration or

dose range, and need to be revised on *in vivo* level, especially in the context of the little correlation that has been found between *in vitro* and *in vivo* studies.[38,39] Therefore, NPs@Glc and NPs@PEG biodistribution and toxicity at short (72 h) and long term (four months) were analyzed employing 6-weeks old Swiss male and female individuals. The injected dose (0.1 mmol Fe/kg animal) was similar to the dose of iron used as contrast agent in clinical magnetic resonance imaging.[40,41]

Intravenous administration of both types of NPs did not affect animal body weight either in short (Fig. S9a) or long term (Fig. S9b) studies. Neither other symptoms of toxicity, effect on organs index (Fig. S10) nor tissue structural changes (Fig. S11 and S12) were found. Finally, four blood chemical parameters related to liver, kidney and muscle function (alanine aminotransferase (ALT), creatinine kinase (CK), creatinine and lactate dehydrogenase (LDH)) were analyzed, finding no significant variation with respect to control values (Fig. S13 and S14). Note that the results were the same for male and female animals in contrast to what it has been reported in other studies, where the toxicity induced by PEG-coated gold NPs was different depending on the animal gender.[42] The rest of studies were only performed on female animals.

NPs biodistribution 72 h post-injection

As the IONPs were coated with a polymer shell modified with a fluorescent dye, their localization in selected organs *ex vivo* could be performed by examination of longitudinal tissue sections using fluorescence microscopy. 72 h after the administration of NPs@Glc, an intense and abundant fluorescence signal evidenced NPs accumulation mainly in the liver and spleen (Fig. 5). Whereas in the liver NPs were distributed homogenously throughout the tissue, in the spleen they were primarily observed in the red pulp and/or marginal zone.[43] Also, a scarce signal

of NPs@Glc was found in the kidneys (Fig. 5). Interestingly, 72 h after administration NPs@PEG were detected in all examined organs (Fig. 5 and Fig. S15). The highest NPs@PEG accumulation was observed in the liver and spleen with homogenous distribution in both organs (Fig. 5) but also a quite significant amount was found in the reproductive organs, in both females and males. NPs@PEG in lower quantities were also localized in the kidneys, lungs, heart and thymus (Fig. S15). Of note, the disparate biodistribution profile for both NPs types could be specially appreciated in the spleen, where NPs@Glc were accumulated only in the red pulp and/or marginal zone, while NPs@PEG were homogenously distributed in the tissue.

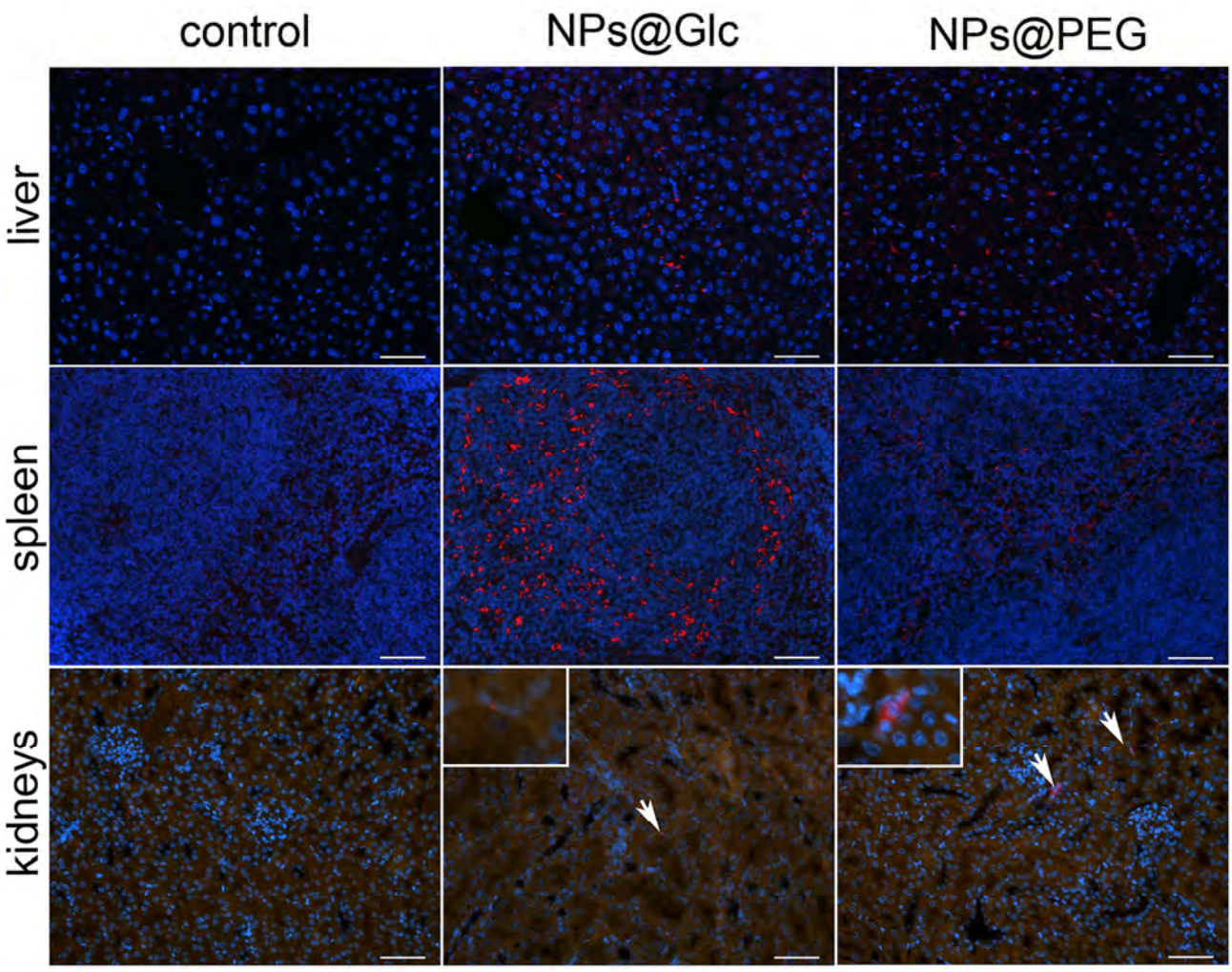

Figure 5. Representative images of the biodistribution of NPs@Glc and NPs@PEG 72 h after administration in mice liver, spleen and kidneys analyzed by fluorescence microscopy *ex vivo*. Both NPs types were found mostly in the liver and spleen. For better visualization of NPs scarcely accumulated in the kidneys tissue (indicated by white arrows and enlarged in the left upper corner of each photo), fluorescence from the red channel has been superimposed with the one from the green channel. Control tissue sections originate from PBS treated mice. Cell nuclei were labeled with DAPI. Scale bar: 50 μm.

Those results were confirmed by the AC magnetic measurements through the analysis of the out-of-phase susceptibility ($\chi''(T)$) profile, which allows to specifically identify and quantify the presence of superparamagnetic material, such as IONPs in biological matrices. In this case other iron-containing species (e.g. hemoglobin or ferritin) that are commonly present in tissue samples, do not contribute to the $\chi''(T)$ signal.[44] This is a huge advantage over traditional methods for IONPs detection, such as elemental analysis or Prussian Blue staining, which fail to accurately quantify very small amount of iron from NPs due to a substantial amount of endogenous iron. As already suggested by the fluorescence microscopy, magnetic measurements confirmed that NPs@Glc were abundantly accumulated in the liver and spleen (Fig. 6a), whereas NPs@PEG were found in all analyzed organs, including lungs and heart (Fig. 6b).

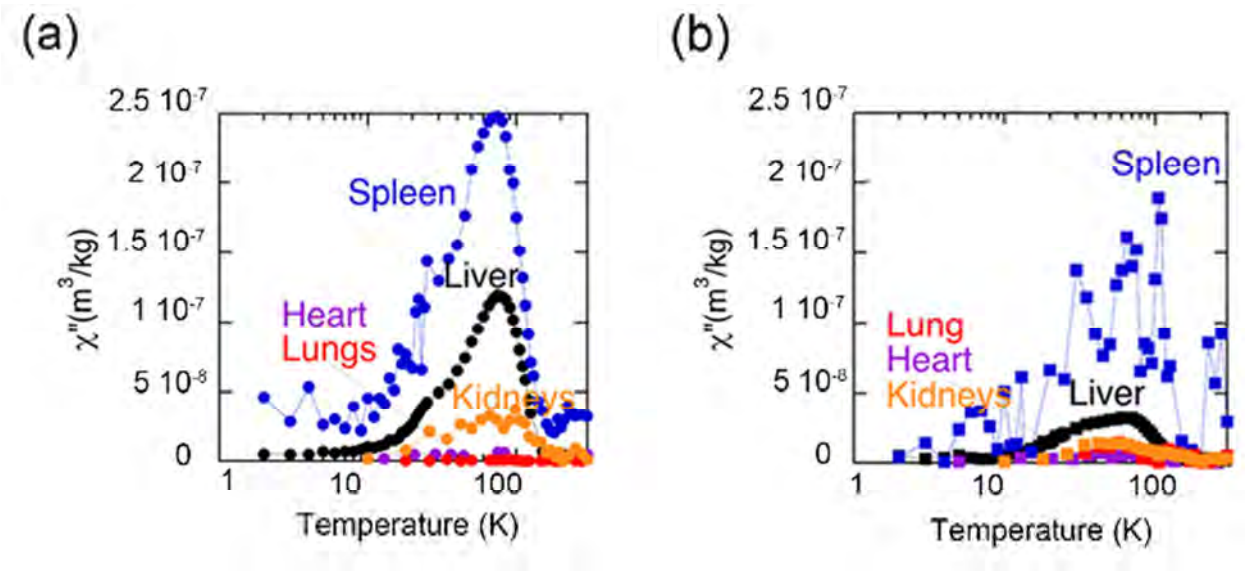

Figure 6. IONPs detection by AC magnetic susceptibility in various tissues from mice 72 h after injection of (A) NPs@Glc. or (B) NPs@PEG.

Additionally, the height of the out-of-phase susceptibility *per* mass of the tissue sample acts as a surrogate of the amount of NPs, therefore the amount of Fe in the tissue can be calculated (Table 1). The abundant accumulation of NPs@Glc in the liver and spleen (3.8 and 1.7 higher in comparison with NPs@PEG, respectively, Table 1), suggests that NPs@Glc were rapidly recognized by macrophages and cleared from the blood, disabling accumulation in other organs. This hypothesis of fast clearance of NPs@Glc from the bloodstream by macrophages is supported by the *in vitro* studies performed with RAW 264.7 macrophages (Fig. S16), in which NPs@Glc and NPs@PEG bearing PC were incubated in serum-free conditions to avoid unspecific adsorption of proteins. If the proteins (i.e. opsonins) adsorbed in the PC are recognized by macrophages, are in the correct orientation and not masked with other proteins, they should be able to bind to macrophage receptors and be uptaken.[45] Just two hours after

incubation we found that while NPs@PEG were not uptaken by the macrophages, NPs@Glc were highly uptaken. This confirms the results of the *in vivo* biodistribution, and has to be related with the different enrichment of proteins in each PC (as the amount of adsorbed proteins is similar), although their different orientation cannot be ruled out. Although coating of NPs with glucose significantly decreases the unspecific adsorption of model proteins[46] and increases NPs uptake by cancerous cells *in vitro* (due to their elevated metabolic growth rate[47] and/or expression of glucose transporters),[48,49] *in vivo* studies demonstrate removal from the blood within an hour,[50] scarce accumulation in the tumor tissue and rapid uptake by the liver and spleen,[51] probably as a result of PC impact.

Interestingly, it has to be highlighted that the composition of PC found *in vitro* where the ratio between albumin/complement proteins was nearly two times higher for NPs@PEG compared with NPs@Glc, positively correlated with the NPs behavior *in vivo* 72 h after injection.

Table 1. Quantification of NPs@Glc and NPs@PEG accumulated in various mice organs 72 h post-injection calculated from the height of the tissue samples χ'' maxima. It has to be taken into account that as the total mass of the liver is several times higher than the spleen, the total amount of iron will be higher in the liver.

	NPs@Glc	NPs@PEG
	mg of Fe *per* kg of lyophilized tissue	
Liver	0,06	0,016
Spleen	0,13	0,08
Kidneys	0,02	0,007
Lungs	-	0,007

Heart	-	0,003

NPs biodistribution four months post-injection

Once NPs are cleared from the blood and accumulated in organs, they undergo biotransformation processes, which may result in their degradation, assimilation and therefore elimination or persistence. Evaluation of NP behavior in a long time frame is necessary to encompass the whole NP lifecycle *in vivo* and predict potential exposure risk. In this case, AC magnetic measurements corroborated the results obtained from the fluorescence examination of tissue sections (Fig. S17 and S18) showing that four months after the injection NPs@Glc were still present in the liver and spleen, whereas NPs@PEG were only present in the liver (Fig. 7). From the rest of the organs, both NPs types were cleared. From the relative height of the $\chi''(T)$ peak at four months, which was always smaller than the peak at 72 h (Fig 7. and Table 2), it was demonstrated that there was a general trend of NPs clearance in both liver and spleen.

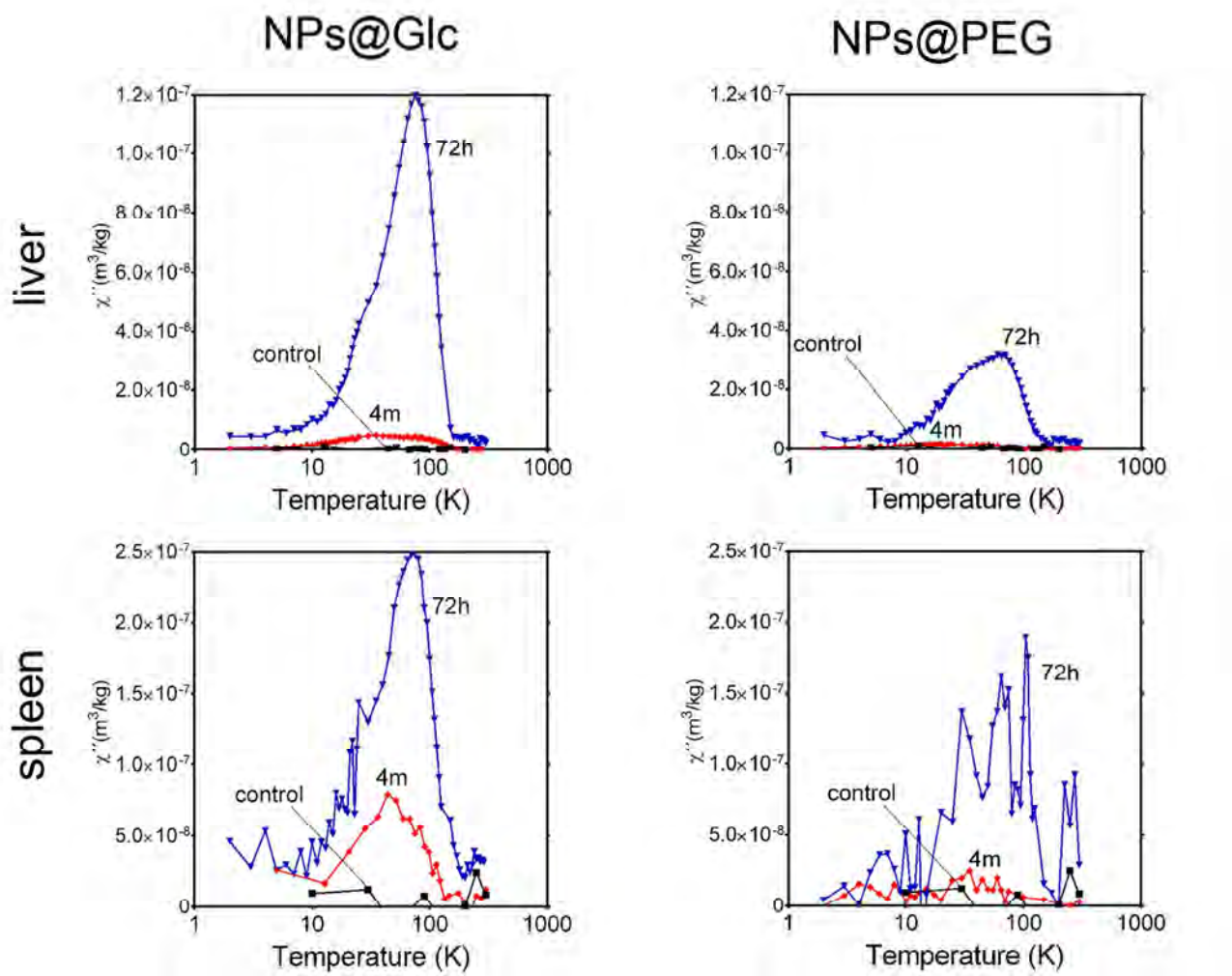

Figure 7. Iron detection by AC magnetic susceptibility in the liver (upper row) and spleen (lower row) 72 h (blue line) and four months (red line) after the injection of NPs@Glc (left column) or NPs@PEG (right column). In all cases, four months after the administration the NPs clearance was detected as the χ″ (T) maximum height decreased in respect to the 72 h one.

The liver showed 23 times fewer NPs@Glc compared to 72 h, while the spleen showed only three times signal reduction. That evidenced that NPs@Glc were cleared more efficiently from the liver than from the spleen. In the case of NPs@PEG, although the maximum χ″(T) for the liver decreased nearly 18 times when compared to 72 h signal, it was still present, whereas for

the spleen it almost disappeared. It is surprising that the degradation process in this case was faster in the spleen than in the liver, more particularly when the concentration in the spleen 72 h post-injection of NPs@PEG was 4.7 times higher compared to the liver.

Table 2. Characteristics of the $\chi''(T)$ maximum for NPs@Glc and NPs@PEG accumulated in various mice organs 72 h and four months post injection.

	$\chi''(T)$ maximum (m^3/kg)			
	NPs@Glc		NPs@PEG	
	72 h	4 months	72h	4 months
Liver	$1.2x10^{-7}$	$5.2x10^{-9}$	$3.2x10^{-8}$	$1.9x10^{-9}$
Spleen	$2.5x10^{-7}$	$7.9x10^{-8}$	$1.5x10^{-7}$	-
Kidneys	$3.7x10^{-8}$	-	$1.4x10^{-8}$	-
Lungs	-	-	$1.5x10^{-8}$	-
Heart	-	-	$6.7x10^{-9}$	-

In summary, both NPs types showed, apart from diverse biodistribution pattern, different clearance rate. Whereas NPs@PEG were more efficiently cleared from the spleen, NPs@Glc clearance was more dynamic in the liver. In fact, faster clearance of NPs from liver has been described for many NPs types irrespectively of their core or coating.[8,52,53] This is explained by the fact that the concentration *per* gram of organ is always higher in the spleen than in the liver. Therefore it is thought that the spleen degradation capacity may be saturated. However, this assumption finds a confirmation here only in the case of NPs@Glc and not NPs@PEG, as the latter were almost totally cleared from the spleen (Fig. 7).

To characterize the biodegradation of the NPs, the shift in temperature of the scaled $\chi''(T)$ maxima was studied (Fig. 8). In the case of NPs@PEG, there was a clear shift of the $\chi''(T)$ maximum from 60 K to 24 K over time (Fig. 8a). This indicates that most of the NPs@PEG in the liver underwent a transformation that could be associated with a reduction of NPs size, disaggregation, or both. In the case of the liver from the animals that received the NPs@Glc, the signal was broader, in particular towards lower temperatures (Fig. 8b). This could be interpreted as a fraction of the NPs being partially degraded while another fraction still remains not modified. In the spleen, NPs@Glc were scarcely transformed, as the maximum was only slightly shifted towards lower temperatures (Fig. 8c).

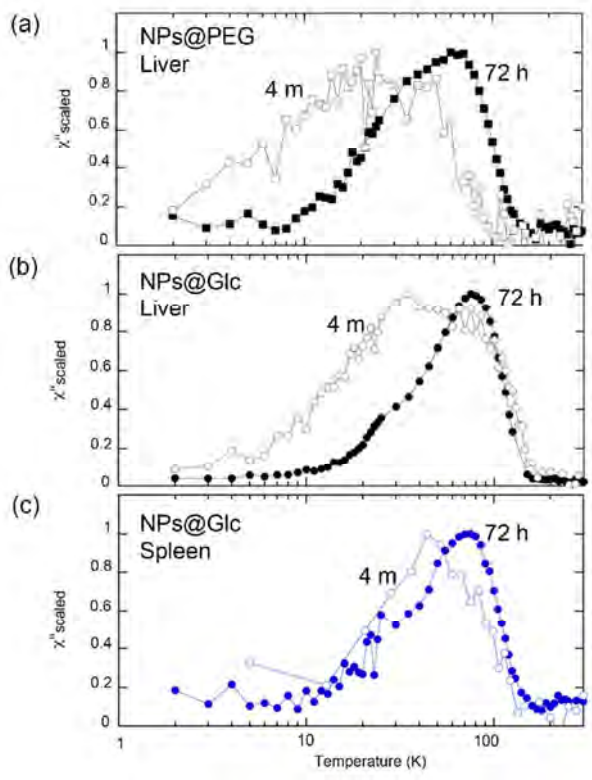

Figure 8. Tissue magnetic characterization. (a)-(c) Temperature dependence of the out-of-phase component of the AC magnetic susceptibility scaled to their maxima. (a) NPs@PEG in the liver, (b) NPs@Glc in the liver and (c) NPs@Glc in the spleen at different post-administration times (72 h and four months).

If in the spleen the core of the NPs@Glc remained barely unmodified during the four months, the decrease of NPs concentration could be related to: i) a different degradation mechanism than in the liver, i.e. a small fraction of NPs are being degraded while the vast majority is unaffected; ii) an excretion of the NPs from the tissue, reducing the amount of NPs but not degrading them.

As seen before, the PC of NP@Glc was enriched in opsonins when compared to the PC of NP@PEG that was more enriched in albumin. The fact that proteins from the PC can be degraded in lysosomes has been previously described.[54] Further, Ma et al.[7] described that the degradation rate of PC is dependent on the type of the protein. Specifically, in this study the protein coronas were formed using human serum albumin, γ-globulin, or serum fibrinogen. Their results indicate that the degradation is fastest for albumin corona and slowest for fibrinogen corona. In this case, NPs@PEG corona is enriched in albumin and therefore *in vivo* could be degraded faster. Further, only the PC of NPs@Glc contained fibrinogen, which could be indicative of a slower rate of degradation.

Although partial degradation of NPs *in vivo* has been already observed in other works, a general trend cannot be ruled out due to the different methodologies, NPs, animal models or the time after injection. For instance, Kolosnijaj-Tabi *et al.*[8] detected by TEM uneven dissolution of some gold-iron heterostructures one year after administration, while other NPs remained untouched,

suggesting that each heterostructure has its own kinetics of degradation. Similarly, when analyzing the biodegradation of iron oxide nanocubes, it was shown that some of them were found degraded already 14 days after injection, where others were untouched.[34] The irregular petal-resemble shape of the heterostructures or unequal polymer shell coverage on the nanocubes edges may facilitate a different cellular medium penetration, leading to inconsistent degradation of the nanomaterial. However, these factors cannot be taken into account in the present study as interestingly differences in degradation have been observed between two NPs containing exactly the same core and polymer shell and differentiated only by the subsequent surface modification.

The fact that *in vivo* NPs@PEG were cleared faster than NPs@Glc and completely transformed whilst *in vitro* where almost unmodified, may result from several reasons: i) *in vitro* the used medium does not exactly reproduce the lysosome conditions; ii) differences in the composition of the PC *in vivo* and *in vitro* that could ultimately affect the degradation rate of both PCs.[7] iii) alternatively, the variation in the degradation rate could be related with the density of NPs in lysosomes. In fact, by TEM examination and X-Ray microanalysis (EDC) of tissue sections NPs@Glc were found to be tightly packed in the lysosomes of the spleen and liver cells on the contrary to NPs@PEG (Fig. 9 and Fig. S19-20). This could ultimately affect the degradation kinetics due to an unequal access of enzymes to the core.[6] Although further research is needed to fully unravel these issues, we have demonstrated that *in vivo* studies are absolutely necessary in order to understand the long term degradation of NPs.

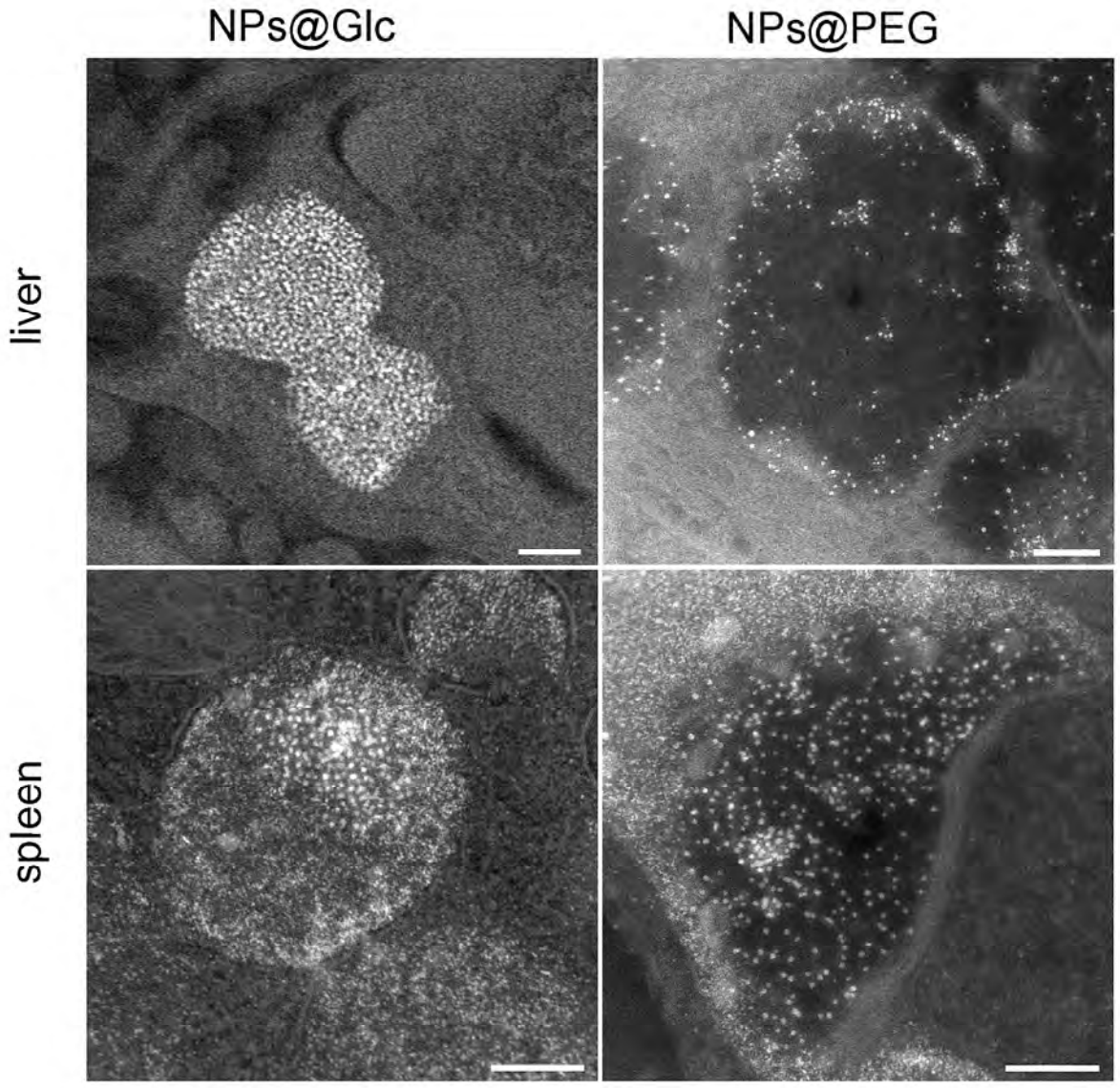

Figure 9. TEM micrographs of liver (upper row) and spleen (lower row) tissue of mice treated with NPs@Glc (left column) and NPs@PEG (right column) acquired in STEM mode. Note that NPs@Glc in both tissues are highly uploaded in vesicles on the contrary to NPs@PEG. Scale bar: 200 nm. STEM: scanning transmission electron microscopy.

CONCLUSIONS

Before employing NPs *in vivo*, the parameters that affect their fate and degradation should be controlled. Using two NPs with identical core but different surface coating, we have shown that biodistribution and degradation over four months are completely different. In this case, a direct correlation between the PC composition *in vitro* and the fate of NPs *in vivo* was established. Moreover, it has been demonstrated that two parameters govern the NPs degradation *in vitro*: the surface coating, which influences the degradation rate, and the PC, which protects against NPs core degradation in acidic conditions.

In vivo, it has been shown that NPs@PEG core suffered a faster degradation over time than NPs@Glc, in both liver and spleen. Interestingly, the degradation kinetics was different in the liver and spleen, depending on the NPs type. Although the degradation rate could be related to overlapping factors, these differences can still have their primary origin in the PC, whose composition drives NPs fate and may also influence on the degradation rate in the lysosomes. For the first time it has been demonstrated that the biodegradation process is not only related with the NPs core and shell, but also with the surface coating, and therefore the associated PC. Further research will increase our understanding of NPs biodegradation associated to PC, opening the way to adopt strategies to control NPs behavior on the long-term frame.

METHODS

Chemicals. Unless otherwise stated, all reagents were purchased from Sigma-Aldrich (MO, USA).

NPs functionalization. Fluorescent NPs were obtained by modifying the PMAO polymer with tetramethylrhodamine 5(6)-carboxamide cadaverine (TAMRA; Anaspec [Seraing, Belgium]). As already reported,[16] 1% of the polymer monomers were modified with TAMRA before transferring the MNPs into water. Functionalization with glucose or PEG (MW = 5000 Da) was performed by incubating 1 mg of Fe with 42 μmol of N-(3-dimethylaminopropyl)-N′-ethylcarbodiimide hydrochloride (EDC), 30 μmol of 4-aminophenyl β-D-glucopyranoside or 12.5 μmol of α-methoxy-ω-amino poly(ethylene glycol) 5000 Da (Iris Biotech GmbH [Marktredwitz, Germany]) in 250 μL of SSB buffer pH 9 (50 mM of boric acid and 50 mM of sodium borate). After 3 h of incubation, the ligand excess was removed by washing the MNPs with phosphate-buffered saline (PBS) pH 7.4 in a centrifugal filter with a membrane of 100 kDa molecular weight limit (Merck Millipore, Darmstadt, Germany).

Protein corona characterization. Protein corona formation. 0.25 mg of Fe of each NP type (NPs@PMAO, NPs@Glc, NPs@PEG) was incubated for 3 h at 37 ºC with 775 μg of serum proteins in a final volume of 500 μL by adding 10 mM HEPES pH 7.4. Afterwards, the samples were washed twice in 500 μL of 10 mM MES pH 7.4 by ultracentrifugation at 18000 × g at 4 ºC for 1 h. The isolation of proteins bound on the NPs was performed by SDS buffer elution protocol.[55] Briefly, after the last wash, NPs were suspended in 250 μL of 1% SDS and 100 mM Tris buffer (pH 7.4) for 1 h at room temperature to elute the bound proteins from the NPs. Then the NPs were removed from the elution buffer *via* centrifugation at 16 000 ×g at 4 ºC for 60 min. About 1 mL of cold acetone was added to the eluent and kept at -20 ºC overnight to precipitate the proteins. After centrifugation and drying the acetone from the tube, the protein pellet was dissolved in 6 M Urea (GE Healthcare, Little Chalfont, UK) and 50 mM ammonium bicarbonate by vortexing and brief sonication.

Digestion procedure. After protein quantification (see the supporting information), 20 µg of each NP bound protein sample was subjected to tryptic digestion. Each protein sample was reduced by 10 mM DTT for 1 h at room temperature, then alkylated with 30 mM IAA for 30 minutes in dark and finally reaction was stopped by the addition of 37.5 mM N-Acetyl-L-cysteine (NAC) for 15 minutes at room temperature. About 2 µg Trypsin Gold, MS Grade (Promega Biotech, Wisconsin, USA) was added to digest proteins overnight at 37 ºC.

Liquid chromatography-Mass spectrometry analysis (LC-MS). Tryptic digests were analyzed using a linear ion trap Velos-Orbitrap mass spectrometer (Thermo Fisher Scientific, Bremen, Germany). Instrument control was performed using Xcalibur software package, version 2.1.0 (Thermo Fisher Scientific, Bremen, Germany). Peptide mixtures were fractionated by on-line nanoflow liquid chromatography using an EASY-nLC system (Proxeon Biosystems, Thermo Fisher Scientific) with a two-linear-column system. Digests were loaded onto a trapping guard column (EASY-column, 2 cm long, ID 100 µm and packed with Reprosil C18, 5 µm particle size from Proxeon, Thermo Fisher Scientific) at a maximum pressure of 160 bar. Then, samples were eluted from the analytical column (EASY-column, 10cm long, ID 75 µm and packed with Reprosil, 3 µm particle size from Proxeon, Thermo Fisher Scientific). Separation was achieved by using a mobile phase from 0.1% FA (Buffer A) and 100 % acetonitrile with 0.1 % FA (Buffer B) and applying a linear gradient from 5 to 35 % of buffer B for 90 min at a flow rate of 300 nL/min. Ions were generated applying a voltage of 1.9 kV to a stainless steel nano-bore emitter (Proxeon, Thermo Fisher Scientific), connected to the end of the analytical column. The LTQ Orbitrap Velos mass spectrometer was operated in data-dependent mode. A scan cycle was initiated with a full-scan MS spectrum (from m/z 300 to 1600) acquired in the Orbitrap with a resolution of 30000. The 20 most abundant ions were selected for collision-induced dissociation

fragmentation in the linear ion trap when their intensity exceeded a minimum threshold of 1000 counts, excluding singly charged ions. Accumulation of ions for both MS and MS/MS scans was performed in the linear ion trap, and the AGC target values were set to 1×10^6 ions for survey MS and 5000 ions for MS/MS experiments. The maximum ion accumulation time was 500 and 200ms in the MS and MS/MS modes, respectively. The normalized collision energy was set to 35%, and one microscan was acquired per spectrum. Ions subjected to MS/MS with a relative mass window of 10 ppm were excluded from further sequencing for 20 s. For all precursor masses a window of 20 ppm and isolation width of 2 Da was defined. Orbitrap measurements were performed enabling the lock mass option (m/z 445.120024) for survey scans to improve mass accuracy.[56]

Protein Identification. LC-MS/MS data was analyzed using the Proteome Discoverer 1.2 software (Thermo Fisher Scientific) to generate mgf files. Processed runs were loaded to ProteinScape software (Bruker Daltonics, Bremen, Germany) and proteins were identified using Mascot (Matrix Science, London UK). MS/MS spectra were searched with a precursor mass tolerance of 10 ppm, fragment tolerance of 0.5 Da, trypsin specificity with a maximum of 2 missed cleavages, cysteine carbamidomethylation set as fixed modification and methionine oxidation as variable modification. Identifications were filtered at 1% False Discovery Rate (FDR) at peptide level.

Signaling pathways analysis. To identify biological functions enriched within our set of unique identified proteins, the UniProt IDs corresponding to exclusive identified proteins adsorbed to NPs@PEG and NPs@Glc were uploaded and mapped into the Ingenuity Pathway Analysis (IPA) software (QIAGEN, Redwood City, CA, USA). The Molecular and Cellular Functions lists were generated and Venn diagram was used to analyze the matching functions

***In vitro* degradation study of NPs.** NPs at equals concentrations (0,1 mg/mL; 46 μg of Fe) were incubated in lysosomal mimicking medium containing citric acid 4.4 mM and sodium citrate tribasic dihydrate 5.6 mM pH 4.7 at room temperature. NPs@Glc and NPs@PEG were incubated for ten days, whereas NPs@PEG for two months. As a control NPs were left for the same period of time in water. Afterwards, all samples were centrifuged at 21920 x g for 1 h at 4 °C. The supernatant was discarded as the NPs were resuspended in water for further TEM, HR-TEM, STEM or AC magnetic measurements. TEM analysis were carried out using a Tecnai T20 (FEI, Netherlands) transmission electron microscope working at 200 kV. HT-TEM analysis was performed on Tecnai F30 (FEI company, Netherlands) transmission electron microscope working in TEM or Scanning-Transmission (STEM) mode and equipped in X-Ray Microanalysis (EDS) which was used for spectroscopy experiment. The magnetic characterization was performed in a Quantum Design MPMS-XL and MPMS-5S SQUID magnetometers equipped with an AC (Alternating Current) magnetic susceptibility option. The NPs were placed in polycarbonate capsules and the measurements were performed with AC amplitude of 0.41 Oe, in the temperature range between 2 and 300 K and at a frequency of 11 Hz.

Animal experimentation. All the experiments carried out on animals were accepted by the Ethics Advisory Committee for Animal Experimentation of the University of Zaragoza and performed according to the institutional animal use and care regulation of the Centro de Investigación Biomédica de Aragón (CIBA; Zaragoza, Spain). The animals were purchased from the CIBA center and fed a standard diet *ad libitum* throughout the experiments. Pathogen-free female 6-week-old Swiss mice (mean weight 29.51±3.12 g) were randomly divided into three different groups: mice injected with NPs@Glc or NPs@PEG, and control group where PBS was

injected. To reach statistically significant results, each group consisted of five animals, experiments were performed using male and female animals and repeated twice. NPs@Glc and NPs@PEG were suspended in 100 µL of PBS and injected intravenously in the tail vein at dose of 0.1 mmol of Fe *per* kg (injected dose 3 µmol/animal). Mice were sacrificed 72 h and four months after the injection in CO_2 gas chamber. Subsequently the blood has been collected by cardiac puncture using 10% of sodium citrate as anticoagulant for plasma separation *via* centrifugation (15 min, 2000 x g). The samples were left to clot at room temperature for 30 min and then, serum were removed and stored at –80 °C for later analyses. ALT (alanine aminotransferase), and CK (creatine kinase), activities were measured according to the IFCC recommendations, by means of the decrease (ALT) or increase (CK) of absorbance at 340 nm. Determination of LDH (lactate dehydrogenase) activity was measured by the transformation of lactate to piruvate, measuring the increase of absorbance at 340 nm. Creatinine concentrations were determined by the Jaffé method. All measurements were carried out using an automated analyzer (Cobas c501, Roche Diagnostics). Finally liver, spleen, kidneys, heart, lungs, thymus and reproductive organs were excised and prepared for fluorescent microscopy examination, histopathological tissue examination (in the ESEM), TEM and AC magnetic measurements.

Fluorescence microscopy examination of tissue sections. NPs localization in tissues of excised organs has been examined by fluorescence microscopy owing to the presence of TAMRA fluorophore coupled to the PMAO polymer surrounding NPs. For that purpose pieces of all before mentioned organs were fixed with pH 7.4 phosphate-buffered 4% paraformaldehyde during 24 h at 4 °C and processed in mesh cassettes (Mesh Biopsy Cassette) using a standard protocol (automatic tissue processor; Tissue-Tek Xpress x50). The preparation of the blocks was carried out with the block making unit (Leica EG1150) after which the blocks were solidified on

a cold plate. Samples were embedded in paraffin, sectioned at three microns thick (Rotary microtome Leica RM2255) and placed in a tempered bath where they were collected with Superfrost slides (Dako Flex IHC Microscope Slides; ref: K8020). The slides were placed in vertical racks and allowed to dry in an oven. Afterwards, a process of dewaxing and hydration was performed for subsequent staining with 4,6-diamidino-2-phenylindole (DAPI). The samples were mounted directly using DAPI - Fluoromount - G (SouthernBiotech; Ref 0100-20) and examined under inverted microscope (Nikon Eclipse Ti-E, Amsterdam, The Netherlands).

TEM characterization of organs. For electron microscopic analysis, the excised organs were cut into 1 mm^3 pieces and fixed with 2.5% glutaraldehyde/2% paraformaldehyde in 0.1 M pH 7.4 sodium phosphate buffer for 24 h at room temperature and subsequently for 5 days at 4 °C. Following, the samples were washed for 30 min four times with sodium phosphate buffer, post-fixed with 2% osmium, rinsed, dehydrated and embedded in Durcupan resin (Fluka, Sigma-Aldrich, St. Louis, USA). Semithin sections (1.5 μm) were cut with an Ultracut UC-6 (Leica, Heidelberg, Germany) and stained lightly with 1% toluidine blue. Finally, ultra-thin sections (0.08 μm) were cut with a diamond knife, stained with lead citrate (Reynolds solution) and examined under a 300 kV transmission electron microscope FEI Tecnai F30 (FEI company, Netherlands) enabling working in STEM mode and performing EDS.

Magnetic characterization of organs. Tissue samples were freeze-dried in Telstar cryodos-50 during 24 h. Pieces of the different tissues were directly placed in gelatin capsules for their magnetic characterization. Spleen samples presented the lowest weights (2.5 – 7.5 mg) while the bigger volume of the livers allowed a bigger amount of tissue to be characterized (88 – 95 mg). The low amount of spleen sample results in noisier magnetic measurements in comparison with the livers.

The magnetic characterization was performed in a Quantum Design MPMS-XL and MPMS-5S SQUID magnetometers equipped with an AC (Alternating current) magnetic susceptibility option. The measurements were performed with AC amplitude of 0.41 Oe, in the temperature range between 2 and 300 K and at a frequency of 11 Hz.

NPs@Glc and NPs@PEG were characterized in the same conditions, by placing a known volume of the injected particles into polycarbonate capsules, in order to use the data as standards for the quantification of the amount of NPs in each tissue. Magnetic nanoparticle quantification in tissue samples was performed following the protocol previously described.[57]

ASSOCIATED CONTENT

Supporting information. Supplementary material (synthesis, functionalization and characterization of the NPs, stability of the NPs in diverse media, further details of the PC study and *in vitro* degradation study, fluorescent examination of tissue sections, *in vivo* toxicity study, EDC of the NPs in the liver and spleen) is available in the online version of this article.

AUTHOR INFORMATION

Corresponding authors:

* Dr. Maria Moros, email: m.moros@isasi.cnr.it

* Dr. Jesus Martinez de la Fuente, email: jmfuente@unizar.es

Author Contributions

The manuscript was written through contributions of all authors. All authors have given approval to the final version of the manuscript. ‡These authors contributed equally

Conflict of interest: The authors declare no competing financial interest.

ACKNOWLEDGEMENTS

This work was supported by Fondo Social de la DGA (grupos DGA), Ministerio de la Economía y Competitividad del Gobierno de España for the public funding of Proyectos I+D+I - Programa Estatal de Investigación, Desarrollo e Innovación Orientada a los Retos de la Sociedad (project n. SAF2014-54763-C2-2-R and SAF2014-54763-C2-1-R) and the ERC-Starting Grant 239931-NANOPUZZLE. M. M. acknowledges financial support from European Union´s Horizon 2020 research and innovation programme under the Marie Skłodowska-Curie grant agreement No. 660228. R. M. F. acknowledges financial support from Universidad de Zaragoza (JIUZ-2014-CIE-03) and European Union´s Horizon 2020 research and innovation programme under the Marie Skłodowska-Curie grant agreement No. 657215. L. G. acknowledges financial support from the Ramón y Cajal subprogram (RYC-2014-15512). We wish to thank The Advanced Microscopy Laboratory (INA-Universidad de Zaragoza) for access to their instrumentation and expertise. Servicio General de Apoyo a la Investigación-SAI, Universidad de Zaragoza is also acknowledged.

REFERENCES

(1) Markides, H.; Rotherham, M.; El Haj, A. J. Biocompatibility and Toxicity of Magnetic Nanoparticles in Regenerative Medicine. *J. Nanomater.* **2012**, *2012*, 1–11.

(2) Duncan, R.; Gaspar, R. Nanomedicine(s) under the Microscope. *Mol. Pharm.* **2011**, *8*, 2101–2141.

(3) Moros, M.; Ambrosone, A.; Stepien, G.; Fabozzi, F.; Marchesano, V.; Castaldi, A.; Tino, A.; de la Fuente, J.; Tortiglione, C. Deciphering Intracellular Events Triggered by Mild Magnetic Hyperthermia in Vitro and in Vivo. *Nanomedicine (Lond.)* **2015**, *10*, 2167–2183.

(4) Anderson, N. L. The Clinical Plasma Proteome: A Survey of Clinical Assays for Proteins in Plasma and Serum. *Clin. Chem.* **2010**, *56*, 177–185.

(5) Walkey, C. D.; Chan, W. C. W. Understanding and Controlling the Interaction of Nanomaterials with Proteins in a Physiological Environment. *Chem. Soc. Rev.* **2012**, *41*, 2780–2799.

(6) Feliu, N.; Docter, D.; Heine, M.; del Pino, P.; Ashraf, S.; Kolosnjaj-Tabi, J.; Macchiarini, P.; Nielsen, P.; Alloyeau, D.; Gazeau, F.; Stauber, RH.; Parak, WJ. In Vivo Degeneration and the Fate of Inorganic Nanoparticles. *Chem. Soc. Rev.* **2016**, *5*, 33–37.

(7) Ma, Z.; Bai, J.; Jiang, X. Monitoring of the Enzymatic Degradation of Protein Corona and Evaluating the Accompanying Cytotoxicity of Nanoparticles. *ACS Appl. Mater. Interfaces* **2015**, *7*, 17614–17622.

(8) Kolosnjaj-Tabi, J.; Javed, Y.; Lartigue, L.; Volatron, J.; Elgrabli, D.; Marangon, I.; Pugliese, G.; Caron, B.; Figuerola, A.; Luciani, N.; Pellegrino, T.; Alloyeau, D.; Gazeau, F. The One Year Fate of Iron Oxide Coated Gold Nanoparticles in Mice. *ACS Nano* **2015**, *9*, 7925–7939.

(9) Kolosnjaj-Tabi, J.; Lartigue, L.; Javed, Y.; Luciani, N.; Pellegrino, T.; Wilhelm, C.; Alloyeau, D.; Gazeau, F. Biotransformations of Magnetic Nanoparticles in the Body. *Nano Today* **2016**.

(10) Sun, S.; Zeng, H.; Robinson, D. B.; Raoux, S.; Rice, P. M.; Wang, S. X.; Li, G. Monodisperse MFe 2 O 4 (M = Fe, Co, Mn) Nanoparticles. *J. Am. Chem. Soc.* **2004**, *126*, 273–279.

(11) Choi, H. S.; Liu, W.; Misra, P.; Tanaka, W.; Zimmer, J. P.; Ipe, B. I.; Bawendi, M. G.; Frangioni, J. V. Renal Clearance of Quantum Dots. *Nat. Biotechnol.* **2007**, *25*, 1165–1170.

(12) Pellegrino, T.; Manna, L.; Kudera, S.; Liedl, T.; Koktysh, D.; Rogach, A. L.; Keller, S.; Rädler, J.; Natile, G.; Parak, W. J. Hydrophobic Nanocrystals Coated with an Amphiphilic Polymer Shell: A General Route to Water Soluble Nanocrystals. *Nano Lett.* **2004**, *4*, 703–707.

(13) Di Corato, R.; Quarta, A.; Piacenza, P.; Ragusa, A.; Figuerola, A.; Buonsanti, R.; Cingolani, R.; Manna, L.; Pellegrino, T. Water Solubilization of Hydrophobic Nanocrystals by Means of Poly(maleic Anhydride-Alt-1-Octadecene). *J. Mater. Chem.* **2008**, *18*, 1991.

(14) Sperling, R. A.; Pellegrino, T.; Li, J. K.; Chang, W. H.; Parak, W. J. Electrophoretic Separation of Nanoparticles with a Discrete Number of Functional Groups. *Adv. Funct. Mater.* **2006**, *16*, 943–948.

(15) Moros, M.; Delhaes, F.; Puertas, S.; Saez, B.; de la Fuente, J. M.; Grazú, V.; Feracci, H. Surface Engineered Magnetic Nanoparticles for Specific Immunotargeting of Cadherin Expressing Cells. *J. Phys. D. Appl. Phys.* **2016**, *49*, 54003.

(16) Moros, M.; Hernáez, B.; Garet, E.; Dias, J. T.; Sáez, B.; Grazú, V.; González-Fernández, Á.; Alonso, C.; de la Fuente, J. M. Monosaccharides versus PEG-Functionalized NPs: Influence in the Cellular Uptake. *ACS Nano* **2012**, *6*, 1565–1577.

(17) Cole, A. J.; David, A. E.; Wang, J.; Galbán, C. J.; Hill, H. L.; Yang, V. C. Polyethylene Glycol Modified, Cross-Linked Starch-Coated Iron Oxide Nanoparticles for Enhanced Magnetic Tumor Targeting. *Biomaterials* **2011**, *32*, 2183–2193.

(18) Prencipe, G.; Tabakman, S. M.; Welsher, K.; Liu, Z.; Goodwin, A. P.; Zhang, L.; Henry, J.; Dai, H. PEG Branched Polymer for Functionalization of Nanomaterials with Ultralong Blood Circulation. *J. Am. Chem. Soc.* **2009**, *131*, 4783–4787.

(19) Gref, R.; Lück, M.; Quellec, P.; Marchand, M.; Dellacherie, E.; Harnisch, S.; Blunk, T.; Müller, R. H. "Stealth" Corona-Core Nanoparticles Surface Modified by Polyethylene

Glycol (PEG): Influences of the Corona (PEG Chain Length and Surface Density) and of the Core Composition on Phagocytic Uptake and Plasma Protein Adsorption. *Colloids Surfaces B Biointerfaces* **2000**, *18*, 301–313.

(20) Xie, B. J.; Xu, C.; Kohler, N.; Hou, Y.; Sun, S. Controlled PEGylation of Monodisperse Fe 3 O 4 Nanoparticles for Reduced Non-Specific Uptake by Macrophage Cells. *Adv. Mater.* **2007**, *19*, 3163–3166.

(21) Walkey, C. D.; Olsen, J. B.; Guo, H.; Emili, A.; Chan, W. C. W. Nanoparticle Size and Surface Chemistry Determine Serum Protein Adsorption and Macrophage Uptake. *J. Am. Chem. Soc.* **2012**, *134*, 2139–2147.

(22) Dobrovolskaia, M. a; Aggarwal, P.; Hall, J. B.; Mcneil, S. E. Preclinical Studies to Understand NP Interaction with the Immune System and Its Potential Effects on NP Biodistribution. *Mol. Pharm.* **2009**, *5*, 487–495.

(23) Naidu, P. S. R.; Norret, M.; Smith, N. M.; Dunlop, S. A.; Taylor, N. L.; Fitzgerald, M.; Iyer, K. S. The Protein Corona of PEGylated PGMA-Based Nanoparticles Is Preferentially Enriched with Specific Serum Proteins of Varied Biological Function. *Langmuir* **2017**, *33*, 12926–12933.

(24) Monopoli, M. P.; Walczyk, D.; Campbell, A.; Elia, G.; Lynch, I.; Baldelli Bombelli, F.; Dawson, K. A. Physical-Chemical Aspects of Protein Corona: Relevance to in Vitro and in Vivo Biological Impacts of Nanoparticles. *J. Am. Chem. Soc.* **2011**, *133*, 2525–2534.

(25) Monopoli, M. P.; Bombelli, F. B.; Dawson, K. a. Nanobiotechnology: Nanoparticle Coronas Take Shape. *Nat. Nanotechnol.* **2011**, *6*, 11–12.

(26) Campagne, M. V. L.; Wiesmann, C.; Brown, E. J. Macrophage Complement Receptors and Pathogen Clearance. *Cell. Microbiol.* **2007**, *9*, 2095–2102.

(27) Aggarwal, P.; Hall, J. B.; McLeland, C. B.; Dobrovolskaia, M. A.; McNeil, S. E. Nanoparticle Interaction with Plasma Proteins as It Relates to Particle Biodistribution, Biocompatibility and Therapeutic Efficacy. *Advanced Drug Delivery Reviews*, 2009, *61*, 428–437.

(28) Schöttler, S.; Becker, G.; Winzen, S.; Steinbach, T.; Mohr, K.; Landfester, K.; Mailänder, V.; Wurm, F. R. Protein Adsorption Is Required for Stealth Effect of Poly(ethylene Glycol)- and Poly(phosphoester)- Coated Nanocarriers. *Nat. Nanotechnol.* **2016**, 372–377.

(29) Freund, B.; Tromsdorf, U. I.; Bruns, O. T.; Heine, M.; Giemsa, A.; Bartelt, A.; Salmen, S. C.; Raabe, N.; Heeren, J.; Ittrich, H.; Reimer, R.; Hohenberg, H.; Schumacher, U.; Weller, H.; Nielsen, P. A Simple and Widely Applicable Method to 59Fe-Radiolabel Monodisperse Superparamagnetic Iron Oxide Nanoparticles for in Vivo Quantification Studies. *ACS Nano* **2012**, *6*, 7318–7325.

(30) Arbab, A. S.; Wilson, L. B.; Ashari, P.; Jordan, E. K.; Lewis, B. K.; Frank, J. A. A Model of Lysosomal Metabolism of Dextran Coated Superparamagnetic Iron Oxide (SPIO) Nanoparticles: Implications for Cellular Magnetic Resonance Imaging. *NMR Biomed.* **2005**, *18*, 383–389.

(31) Ruiz, A.; Gutiérrez, L.; Cáceres-Vélez, P. R.; Santos, D.; Chaves, S. B.; Fascineli, M. L.; Garcia, M. P.; Azevedo, R. B.; Morales, M. P. Biotransformation of Magnetic Nanoparticles as a Function of Coating in a Rat Model. *Nanoscale* **2015**, *7*, 16321–16329.

(32) Martín, M.; Rodríguez-Nogales, A.; Garcés, V.; Gálvez, N.; Gutiérrez, L.; Gálvez, J.; Rondón, D.; Olivares, M.; Dominguez-Vera, J. M. Magnetic Study on Biodistribution and Biodegradation of Oral Magnetic Nanostructures in the Rat Gastrointestinal Tract. *Nanoscale* **2016**, *8*, 15041–15047.

(33) Gutiérrez, L.; Romero, S.; da Silva, G. B.; Costo, R.; Vargas, M. D.; Ronconi, C. M.; Serna, C. J.; Veintemillas-Verdaguer, S.; del Puerto Morales, M. Degradation of Magnetic Nanoparticles Mimicking Lysosomal Conditions Followed by AC Susceptibility. *Biomed. Eng. / Biomed. Tech.* **2015**, *60*, 417–425.

(34) Lartigue, L.; Alloyeau, D.; Kolosnjaj-Tabi, J.; Javed, Y.; Guardia, P.; Riedinger, A.; Péchoux, C.; Pellegrino, T.; Wilhelm, C.; Gazeau, F. Biodegradation of Iron Oxide Nanocubes: High-Resolution in Situ Monitoring. *ACS Nano* **2013**, *7*, 3939–3952.

(35) Mazuel, F.; Espinosa, A.; Luciani, N.; Reffay, M.; Le Borgne, R.; Motte, L.; Desboeufs,

K.; Michel, A.; Pellegrino, T.; Lalatonne, Y.; Wilhelm, C. Massive Intracellular Biodegradation of Iron Oxide Nanoparticles Evidenced Magnetically at Single-Endosome and Tissue Levels. *ACS Nano* **2016**, *10*, 7627–7638.

(36) Lévy, M.; Lagarde, F.; Maraloiu, V.-A.; Blanchin, M.-G.; Gendron, F.; Wilhelm, C.; Gazeau, F. Degradability of Superparamagnetic Nanoparticles in a Model of Intracellular Environment: Follow-up of Magnetic, Structural and Chemical Properties. *Nanotechnology* **2010**, *21*, 395103.

(37) Bertoli, F.; Garry, D.; Monopoli, M. P.; Salvati, A.; Dawson, K. A. The Intracellular Destiny of the Protein Corona : A Study on Its Cellular Internalization and Evolution. *ACS n* **2016**, *10*.

(38) NDong, C.; Tate, J. A.; Kett, W. C.; Batra, J.; Demidenko, E.; Lewis, L. D.; Hoopes, P. J.; Gerngross, T. U.; Griswold, K. E. Tumor Cell Targeting by Iron Oxide Nanoparticles Is Dominated by Different Factors in Vitro versus in Vivo. *PLoS One* **2015**, *10*, 1–18.

(39) Sayes, C. M.; Reed, K. L.; Warheit, D. B. Assessing Toxicology of Fine and Nanoparticles: Comparing in Vitro Measurements to in Vivo Pulmonary Toxicity Profiles. *Toxicol. Sci.* **2007**, *97*, 163–180.

(40) Kalambur, V. S.; of Minnesota, U. *Biotransport of Iron Oxide Magnetic Nanoparticles for Biomedical Applications*; University of Minnesota, 2007.

(41) Barh, D.; Carpi, A.; Verma, M.; Gunduz, M. *Cancer Biomarkers: Minimal and Noninvasive Early Diagnosis and Prognosis*; CRC Press, 2014.

(42) Chen, J.; Wang, H.; Long, W.; Shen, X.; Wu, D.; Song, S. S.; Sun, Y. M.; Liu, P. X.; Fan, S.; Fan, F.; Zhang, XD. Sex Differences in the Toxicity of Polyethylene Glycol-Coated Gold Nanoparticles in Mice. *Int. J. Nanomedicine* **2013**, *8*, 2409–2419.

(43) Taylor, P. R.; Martinez-Pomares, L.; Stacey, M.; Lin, H.-H.; Brown, G. D.; Gordon, S. Macrophage Receptors and Immune Recognition. *Annu. Rev. Immunol.* **2005**, *23*, 901–944.

(44) Mejías, R.; Gutiérrez, L.; Salas, G.; Pérez-Yague, S.; Zotes, T. M.; Lázaro, F. J.; Morales, M. P.; Barber, D. F. Long Term Biotransformation and Toxicity of Dimercaptosuccinic Acid-Coated Magnetic Nanoparticles Support Their Use in Biomedical Applications. *J. Control. Release* **2013**, *171*, 225–233.

(45) Corbo, C.; Molinaro, R.; Taraballi, F.; Furman, N. E. T.; Hartman, K. A.; Sherman, M. B.; Rosa, E. De; Kirui, D. K.; Salvatore, F.; Tasciotti, E. Unveiling the in Vivo Protein Corona of Circulating Leukocyte-like Carriers. *ACS Nano* **2017**, *11*, 3262–3273.

(46) Moros, M.; Pelaz, B.; López-Larrubia, P.; García-Martin, M. L.; Grazú, V.; de la Fuente, J. M. Engineering Biofunctional Magnetic Nanoparticles for Biotechnological Applications. *Nanoscale* **2010**, *2*, 1746–1755.

(47) Vander Heiden, M.; Cantley, L.; Thompson, C. Understanding the Warburg Effect: The Metabolic Requiremetns of Cell Proliferation. *Science (80-.).* **2009**, *324*, 1029–1033.

(48) Venturelli, L.; Nappini, S.; Bulfoni, M.; Gianfranceschi, G.; Dal Zilio, S.; Coceano, G.; Del Ben, F.; Turetta, M.; Scoles, G.; Vaccari, L.; Cesselli, D.; Cojoc, D.. Glucose Is a Key Driver for GLUT1-Mediated Nanoparticles Internalization in Breast Cancer Cells. *Sci. Rep.* **2016**, *6*, 21629.

(49) Kong, T.; Zeng, J.; Wang, X.; Yang, X.; Yang, J.; McQuarrie, S.; McEwan, A.; Roa, W.; Chen, J.; Xing, J. Z. Enhancement of Radiation Cytotoxicity in Breast-Cancer Cells by Localized Attachment of Gold Nanoparticles. *Small* **2008**, *4*, 1537–1543.

(50) Geng, F.; Xing, J. Z.; Chen, J.; Yang, R.; Hao, Y.; Song, K.; Kong, B. Pegylated Glucose Gold Nanoparticles for Improved in-Vivo Bio-Distribution and Enhanced Radiotherapy on Cervical Cancer. *J. Biomed. Nanotechnol.* **2014**, *10*, 1205–1216.

(51) Fahrenholtz, C. D.; Hadimani, M.; King, S. B.; Torti, S. V; Singh, R. Targeting Breast Cancer with Sugar-Coated Carbon Nanotubes. *Nanomedicine (Lond).* **2015**, *10*, 1–18.

(52) Levy, M.; Luciani, N.; Alloyeau, D.; Elgrabli, D.; Deveaux, V.; Pechoux, C.; Chat, S.; Wang, G.; Vats, N.; Gendron, F.; Factor, C.; Lotersztajn, S.; Luciani, A.; Wilhelm, C.; Gazeau F. Long Term in Vivo Biotransformation of Iron Oxide Nanoparticles.

Biomaterials **2011**, *32*, 3988–3999.

(53) Kolosnjaj-Tabi, J.; Di Corato, R.; Lartigue, L.; Marangon, I.; Guardia, P.; Silva, A. K. A.; Luciani, N.; Clément, O.; Flaud, P.; Singh, J. V; Decuzzi, P.; Pellegrino, T.; Wilhelm, C.; Gazeau, F. Heat-Generating Iron Oxide Nanocubes: Subtle "Destructurators" of the Tumoral Microenvironment. *ACS Nano* **2014**, *8*, 4268–4283.

(54) Chanana, M.; Rivera-gil, P.; Correa-Duarte, M. A.; Liz-Marzán, L. M.; Parak, W. J. Physicochemical Properties of Protein-Coated Gold Nanoparticles in Biological Fluids and Cells before and after Proteolytic Digestion. *Angew. Chemie - Int. Ed.* **2013**, *52*, 4179–4183.

(55) Zhang, H.; Burnum, K. E.; Luna, M. L.; Petritis, B. O.; Kim, J.; Qian, W.; Moore, R. J.; Heredia-langner, A.; Thrall, B. D.; Camp, D. G. II.; Smith, RD.; Pounds, JG.; Liu, T. Quantitative Proteomics Analysis of Adsorbed Plasma Proteins Classifies Nanoparticles with Different Surface Properties and Size. *Proteomics* **2012**, *11*, 4569–4577.

(56) Villarreal, L.; Méndez, O.; Salvans, C.; Gregori, J.; Baselga, J.; Villanueva, J. Unconventional Secretion Is a Major Contributor of Cancer Cell Line Secretomes. *Mol. Cell. Proteomics* **2013**, *12*, 1046–1060.

(57) Gutiérrez, L.; Morales, M. P.; Lázaro, F. J. Prospects for Magnetic Nanoparticles in Systemic Administration: Synthesis and Quantitative Detection. *Phys. Chem. Chem. Phys.* **2014**, *16*, 4456–4464.

Graphic for manuscript

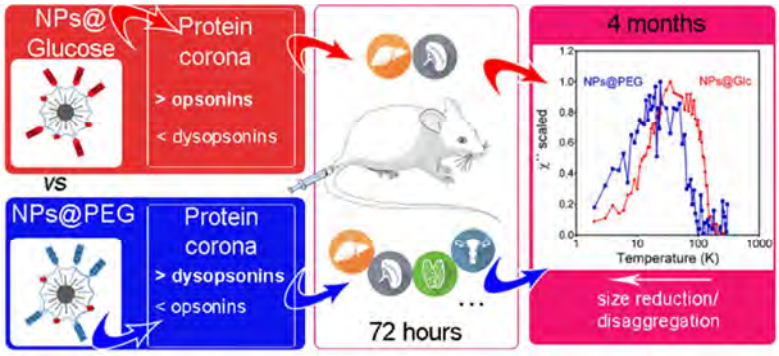
NPs@ Glucose
Protein corona
> opsonins
< dysopsonins
vs
NPs@PEG
Protein corona
> dysopsonins
< opsonins
72 hours
4 months
NPs@PEG
NPs@Glc
χ'' scaled
Temperature (K)
size reduction/ disaggregation